Journal of Materials Chemistry C

ROYAL SOCIETY OF CHEMISTRY

PAPER

View Article Online
View Journal | View Issue

Cite this: *J. Mater. Chem. C*, 2021, **9**, 2912

High-pressure structural phase transition and metallization in Ga_2S_3 under non-hydrostatic and hydrostatic conditions up to 36.4 GPa†

Linfei Yang,‡[a] Jianjun Jiang,‡[b] Lidong Dai,*[b] Haiying Hu,*[b] Meiling Hong,[ac] Xinyu Zhang,[ac] Heping Li[a] and Pengfei Liu[d]

Received 23rd December 2020,
Accepted 19th January 2021

DOI: 10.1039/d0tc06004f

rsc.li/materials-c

The vibrational, electrical and structural properties of gallium sulfide (Ga_2S_3) were explored by Raman spectroscopy, electrical conductivity measurements, high-resolution transmission electron microscopy and first-principles theoretical calculations under different pressure environments up to 36.4 GPa. Upon compression, Ga_2S_3 underwent a first-order structural phase transition accompanied by a semiconductor-to-metal transformation at 17.2 GPa under non-hydrostatic conditions, whereas, the transition occurred at a much lower pressure of 11.3 GPa under hydrostatic conditions because of the influence of the pressure medium. Upon decompression, two possible new high-pressure polymorphs were observed at 8.0 and 3.0 GPa under non-hydrostatic conditions, and similar transition points were obtained under hydrostatic conditions. The structural and electrical transport evolution for Ga_2S_3 upon compression and decompression can help us to deeply understand the high-pressure behaviors of other similar A_2B_3-type structural compounds.

Introduction

In recent decades, A_2B_3-type chalcogenides have attracted widespread research interest owing to their unique physical–chemical properties for use in three-dimensional topological insulators and potential industrial applications in quantum computation and quantum magnetoresistance.[1–6] Pressure can tune the atomic position and electronic structure of the A_2B_3-type chalcogenides away from their original state, and induce remarkable physical phenomena, such as electronic topological transition (ETT), structural phase transitions, metallization and superconductivity.[7–15] As a representative member of the A_2B_3-type families, Ga_2S_3 crystallizes into a stable monoclinic structure with a *Cc* space group under ambient conditions, which exhibits a semiconducting behavior with a wide band gap of 2.8 eV.[16] Investigations of its high-pressure behavior are important in the search for new materials with unique physical properties.

To our knowledge, only one previous high-pressure study reported the phase stability of Ga_2S_3 and its corresponding crystalline structure up to 30.5 GPa using synchrotron X-ray diffraction, X-ray absorption near edge structure measurements and first-principles theoretical calculations.[17] Their results indicated that monoclinic Ga_2S_3 transformed to a new polymorph with a rhombohedral structure ($R\bar{3}m$, $Z = 3$) at 16.0 GPa, and this new high-pressure phase was predicted to exhibit a metallic behavior. Although their theoretical calculation predicted the pressure-induced metallization in Ga_2S_3, it still needs to be checked by reliable experimental evidence. Additionally, the $R\bar{3}m$ phases in other similar compounds of Bi_2Se_3, Bi_2Te_3 and Sb_2Te_3 underwent a pressure-induced ETT at 3–5 GPa.[18–20] Thus, it is noteworthy to investigate whether the $R\bar{3}m$ phase in Ga_2S_3 shows a similar ETT at high pressure. In recent work, the pressure environment has been reported to be a critical influential factor in changing the physical properties of As_2Te_3.[21] As a typical A_2B_3-type chalcogenide for Ga_2S_3, the effect of a pressure environment on its structural and electrical properties remains unclear, and requires more comprehensive investigation.

In the present studies, we investigated the influence of the pressure environment on the high-pressure behavior of Ga_2S_3 using Raman scattering spectroscopy, electrical conductivity measurements, high-resolution transmission electron microscopy

[a] *Key Laboratory of High-Temperature and High-Pressure Study of the Earth's Interior, Institute of Geochemistry, Chinese Academy of Sciences, Guiyang, Guizhou 550081, China. E-mail: dailidong@vip.gyig.ac.cn, huhaiying@mail.gyig.ac.cn*
[b] *Shandong Provincial Key Laboratory of Water and Soil Conservation and Environmental Protection, College of Resources and Environment Sciences, Linyi University, Linyi 276000, China*
[c] *University of Chinese Academy of Sciences, Beijing 100049, China*
[d] *State Key Laboratory of Structural Chemistry, Fujian Institute of Research on the Structure of Matter, Chinese Academy of Sciences, Fuzhou, Fujian 350002, China*

† Electronic supplementary information (ESI) available. See DOI: 10.1039/d0tc06004f

‡ These authors contributed equally to this work.

and the first-principles theoretical calculations up to 36.4 GPa. Our results indicated that Ga_2S_3 underwent a pressure-driven structural phase transition with metallization at 17.2 GPa under non-hydrostatic conditions, and this transition point was lower by 5.9 GPa under hydrostatic conditions. And furthermore, the structural phase transition and metallization in Ga_2S_3 under high pressure are discussed in detail.

Experimental

High-purity Ga_2S_3 (99.99%) was obtained from the Leshan Kaiyada Company, Chengdu, China. The sample was ground to a micron-scale powder in an agate mortar, and baked in a muffle furnace at 323 K for 2 h to avoid the influence of adsorbed water on the physical properties of the sample during the measurements. The microscopic structure for the initial sample was revealed by high-resolution transmission electron microscopy (HRTEM) images, which were collected using a Tecnai G2 F20 S-TWIN TMP. Fig. S1 (ESI†) shows the HRTEM and corresponding fast Fourier transform (FFT) images of the initial sample. We obtained three different crystalline planes of Ga_2S_3, namely (221), (23−2) and (01−3), and their corresponding plane distances were 0.193, 0.185 and 0.189 nm, respectively. A series of bright diffraction spots indicated that the initial sample possessed a high crystallinity.

High-pressure Raman spectroscopy measurements were conducted at room temperature in a piston-type diamond anvil cell (DAC). The anvil culet of two symmetrical diamonds was 300 μm in diameter, and a high pressure was achieved by manually tightening four pressurization screws on top of the DAC equipment. A small piece of the sample was loaded into a 100 μm hole in a T-301 stainless steel gasket (5 mm × 5 mm), and a 5 μm ruby crystal was placed next to the sample as the pressure calibration material. The ruby pressure calibration equation proposed by Mao *et al.*[22] was used to calculate the pressure value in the sample chamber. The pressure calibration of the ruby had a good accuracy (<5% for non-hydrostatic conditions and <3% for hydrostatic conditions). Helium was selected as the pressure medium for all hydrostatic experiments, and no pressure medium was used for the non-hydrostatic measurements. Raman spectra were collected in the frequency range of 100–600 cm^{-1} using a micro-confocal Raman spectrometer (Renishaw 2000). A 514.5 nm Ar^{3+} laser device was used to produce a laser beam, and the beam spot size was ~5 μm. An appropriate laser power of 20 mW was used to avoid overheating and sample destruction. All acquired Raman spectra were well-fitted *via* the Gauss function using Origin software.

High-pressure electrical conductivity measurements were carried out using a four column-type DAC. Owing to the advantage of the four column-type DAC apparatus with a relative lateral window, it can be applied extensively to high-pressure electrical conductivity measurements.[23,24] To prevent the influence of impurity pollution on samples during the electrical conductivity measurements, we did not use a pressure medium in our electrical conductivity experiments for Ga_2S_3. An insulating sample chamber is vital for the electrical conductivity measurements; details of its manufacture have been described in our previous work.[25–28] The AC impedance spectra were obtained using a Solartron-1260 impedance/gain phase analyzer at 10^{-1}–10^{7} Hz. For the temperature-dependent electrical conductivity experiment, a low-temperature environment was achieved by the volatilization of liquid nitrogen, which overwhelmed the DAC device. A K-type thermocouple was mounted on the edge of the bottom diamond to measure the temperature in the pressure chamber and the estimated accuracy was ~5 K.

By using density functional theory (DFT), the structural and electronic evolutions for Ga_2S_3 under high pressure were predicted through the first-principles theoretical calculations, which were conducted by using the CASTEP code within the Material Studio package. The crystal structure of Ga_2S_3 was optimized to reach the lowest total energy using the generalized gradient approximation (GGA) function. In terms of the initial atomic position and crystal parameter for the monoclinic Ga_2S_3 (*Cc*) and rhombohedral phase ($R\bar{3}m$), we used the data reported by Lai *et al.*[17] to implement the first-principles theoretical calculations. For the *Cc* structure, a 6 × 6 × 6 Monkhorst–Pack *K*-point grid was used for the relaxation and density of states (DOS) calculations, and the cutoff energy was 500 eV. For the $R\bar{3}m$ phase, we set the *K*-point grid and cutoff energy to 4 × 4 × 4 and 300 eV, respectively.

Results and discussion

Raman spectroscopy is a traditional method for investigating the high-pressure behavior of A_2B_3-type chalcogenides, which can efficiently detect atomic rearrangements in the crystal structure and subtle structural changes in a nondestructive way. In the present studies, the vibrational property of Ga_2S_3 was explored under different pressure conditions up to 36.4 GPa. Under ambient conditions, as given in Fig. S2 (ESI†), approximately fourteen Raman-active peaks were well-resolved from Raman spectra: 117.3, 143.4, 149.7, 159.9, 235.6, 283.0, 309.0, 330.6, 344.0, 350.9, 368.5, 389.1, 407.3 and 424.4 cm^{-1}. Three primary peaks were located at 117.3, 235.6 and 389.1 cm^{-1}, which can be ascribed to $\nu_s(E)$, $\nu_s(A_1)$ and $\nu_d(F_2)$ of the GaS_4 tetrahedra, respectively.[29] All obtained Raman vibrational modes agree with previous data.[30]

Fig. 1a shows the high-pressure Raman spectra of Ga_2S_3 up to 36.4 GPa during compression under non-hydrostatic conditions. On the basis of the pressure dependence of the frequencies of Raman modes, three different regions are distinguished in Fig. 1b: (i) at 0–15.1 GPa, all Raman modes shifted gradually to higher frequencies with an increase in pressure, but peaks at 309.0, 350.9 and 424.4 cm^{-1} were not detected due to the weak peak intensity; (ii) at 17.2–19.3 GPa, most Raman modes disappeared except for the ν_s (284.3 cm^{-1}), ν_d (389.4 cm^{-1}) and ν_d (426.4 cm^{-1}) bands, and four new peaks denoted M1, M2, M3, and M4 emerged. (iii) At 21.6–36.4 GPa, four new Raman bands were observed in the Raman spectra,

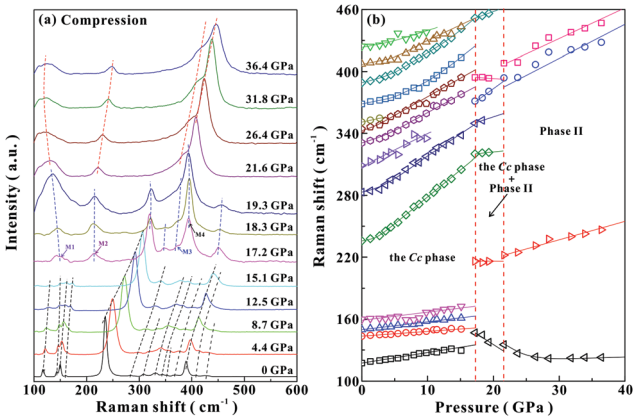

Fig. 1 (a) High-pressure Raman spectra of Ga_2S_3 at various pressure points upon compression under non-hydrostatic conditions. (b) The evolution of Raman modes with the increase of pressure under non-hydrostatic conditions.

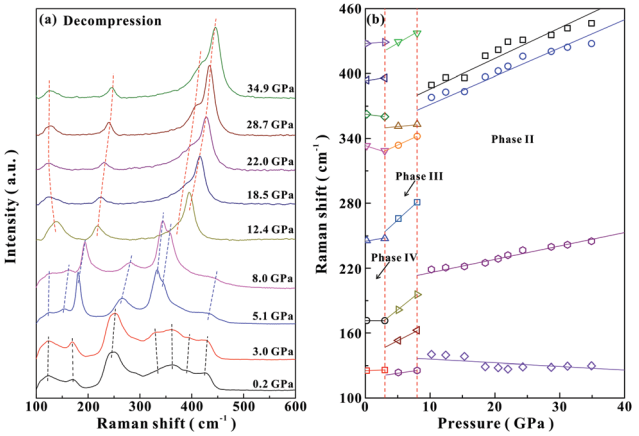

Fig. 2 (a) Raman spectra of Ga_2S_3 obtained in the process of decompression under non-hydrostatic conditions. (b) The pressure dependence of the wave number of Raman vibrational modes in the decompression run under non-hydrostatic conditions.

and the vibrational peaks of the original Ga_2S_3 phase disappeared completely. The occurrence of new Raman peaks at 17.2 GPa provides important evidence to support a pressure-induced structural phase transition in Ga_2S_3. This new high-pressure polymorphe (denoted by phase II) was resolved to an α-Bi_2Te_3-type rhombohedral structure with the space group of $R\bar{3}m$ from previous X-ray experiments by Lai *et al.*[17] The transition point determined in this study is in good agreement with their data at 16.0 GPa. In addition, our Raman results indicated that monoclinic Ga_2S_3 (Cc) coexisted with the new rhombohedral phase ($R\bar{3}m$) over the pressure range of 17.2–19.3 GPa, and this transition was completed above 21.6 GPa. Recent Raman studies on Bi_2Se_3, Bi_2Te_3 and Sb_2Te_3 with the $R\bar{3}m$ structure showed that all of them underwent an ETT under high pressure, which was characterized by the changes in the pressure coefficient of Raman modes.[8,31,32] However, for the $R\bar{3}m$ phase of Ga_2S_3, no anomalies were observed in the pressure dependence of Raman modes at 21.6–36.4 GPa, which implies the absence of ETT in $R\bar{3}m$ Ga_2S_3.

Fig. 2a and b presents the typical Raman spectra and the corresponding pressure-dependent Raman modes of Ga_2S_3 during decompression under non-hydrostatic conditions. Two obvious inflection points occurred at 8.0 and 3.0 GPa, respectively. At 8.0 GPa, Raman characteristic peaks for the $R\bar{3}m$ phase of Ga_2S_3 disappeared suddenly, and seven new peaks were obtained at 125.5, 162.5, 195.4, 280.8, 342.0, 353.1 and 437.3 cm^{-1}, respectively. With further decompression to 3.0 GPa, another new Raman spectrum was collected and seven new peaks were resolved to 126.0, 171.3, 247.5, 328.6, 360.2, 395.8 and 428.9 cm^{-1}. The Raman spectra collected at 8.0 and 3.0 GPa do not belong to any known polymorphs of Ga_2S_3, which indicates that the high-pressure phase of Ga_2S_3 with a $R\bar{3}m$ structure transforms into two new polymorphs (marked by phases III and IV) with an unknown crystal structure upon decompression. Under hydrostatic conditions, as shown in Fig. 3a, our Raman scattering results indicate that a structural phase transition appeared at 11.3 GPa and was completed over 15.9 GPa under

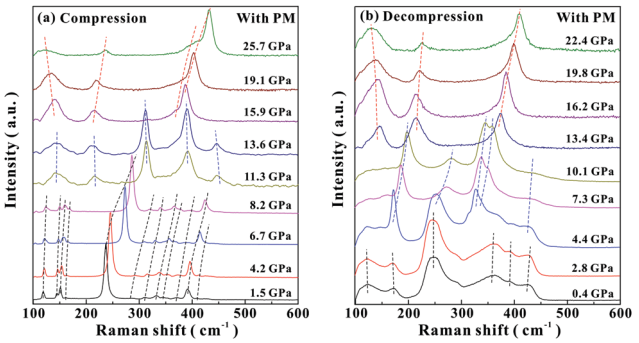

Fig. 3 (a) High-pressure Raman spectra of Ga_2S_3 upon compression under hydrostatic conditions. (b) Raman spectra of Ga_2S_3 upon decompression from 22.4 to 0.4 GPa under hydrostatic conditions.

compression. It makes clear that the phase transition point under non-hydrostatic conditions was much higher than that under hydrostatic conditions, which may be attributed to a large pressure hysteresis effect for the phase transformation. We believe that the presence of a pressure medium would greatly weaken the deviatoric stress in the sample chamber and promote the occurrence of the structural phase transition. During decompression under non-hydrostatic conditions, two phase transitions were also observed at similar pressures of 10.1 and 2.8 GPa (Fig. 3b).

Changes in the crystal structure are often accompanied by detectable variations in the electronic structure. The high-pressure and room-temperature electrical conductivity measurements for Ga_2S_3 were conducted up to 31.4 GPa to reveal the evolution of its electronic structure with pressure. Typical impedance spectra of Ga_2S_3 under high pressure are presented in Fig. 4a–c, which can be divided into three distinct parts: (i) at 2.7–15.1 GPa, the impedance spectra were located at the first quadrant, and three approximate semicircles were distinguished in different frequency ranges, which were attributed to the

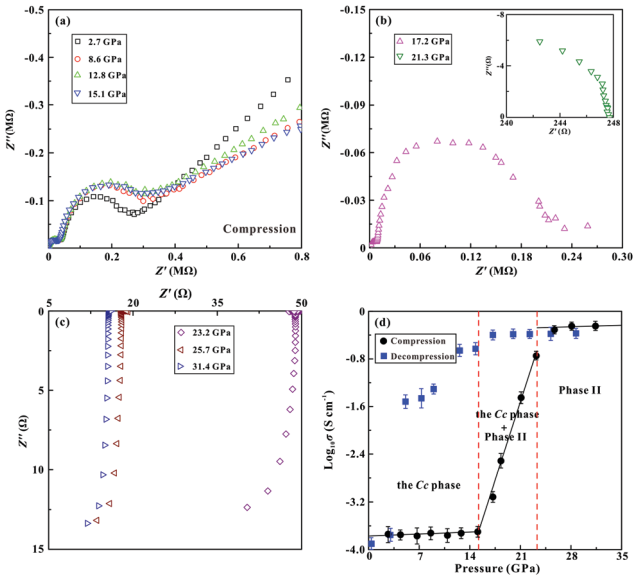

Fig. 4 (a–c) Typical impedance spectra of Ga_2S_3 at 2.7–31.4 GPa in the frequency region of 10^{-1}–10^{7} Hz upon compression. (d) The electrical conductivity of Ga_2S_3 as a function of pressure upon compression and decompression.

contributions of the grain interior, grain boundary and sample–electrode interface, respectively; (ii) at 17.2–21.3 GPa, only the bulk and boundary conduction appeared in the impedance spectra; and (iii) at 23.2–31.4 GPa, all impedance spectra lay in the fourth quadrant in the form of an oblique line. Fig. 4d shows the relationship between the electrical conductivity of Ga_2S_3 and pressure at room temperature; two critical pressure points were 17.2 and 23.2 GPa. From 2.7 to 15.1 GPa, the electrical conductivity was independent of pressure with an almost constant value of 1.78×10^{-4} S cm^{-1}. As the pressure was increased to 17.2 GPa, the electrical conductivity increased to 7.68×10^{-4} S cm^{-1}, and then increased rapidly from 17.2 to 21.3 GPa with a large slope of 0.375 S cm^{-1} GPa^{-1}. Upon further compression from 23.2 to 31.4 GPa, the electrical conductivity reached 0.56 S cm^{-1} and remained stable. For the first transition point at 17.2 GPa, the changes in impedance spectra and slope of the electrical conductivity indicate that the semiconductor Ga_2S_3 (*Cc*) changed to an intermediate state at this pressure point. According to the results of our Raman experiments, the intermediate state belongs to a mixture of monoclinic Ga_2S_3 (*Cc*) and the high-pressure rhombohedral phase ($R\bar{3}m$). At 23.2 GPa, the observed anomalies in the electrical conductivity in the impedance spectra are associated with the transformation from the intermediate state to a single $R\bar{3}m$ phase. Furthermore, the relatively high electrical conductivity above 23.2 GPa and the weak pressure dependence are typical features for metallic material, and thus, it is inferred that the high-pressure $R\bar{3}m$ polymorph is a metallic phase. During decompression, two discontinuous points in the pressure dependence of electrical conductivity occurred at 9.0 and 3.0 GPa, respectively (Fig. S3, ESI†). The pressure points agree well with those determined by our above-mentioned Raman experiments, which further verifies the occurrence of two possible structural phase transitions in Ga_2S_3 upon decompression.

Fig. 5 shows the temperature dependence of electrical conductivity for Ga_2S_3 at a series of pressure points. Typically, the semiconductors are characterized by the positive relationship between the electrical conductivity and temperature, whereas the metal exhibits the opposite relations.[33] At pressures of 7.0 and 12.1 GPa, the electrical conductivity of Ga_2S_3 drastically increased with an increase of temperature, which indicates a semiconducting behaviour for the monoclinic phase (Fig. 5a). At 18.3 GPa, the curve of electrical conductivity had a positive slope in the low-temperature region, but the curve in the high-temperature range exhibited a negative slope, which implies the coexistence of semiconductor and metallic phases (Fig. 5b). At 21.5, 25.1 and 30.2 GPa, the electrical conductivity decreased gradually over the temperature range, which reflects the completion of semiconductor-to-metal transition (Fig. 5c). The transition pressure point of the metallization agreed well with that of the structural phase transition in Ga_2S_3, and therefore, we believe that the semiconductor-to-metal transition is caused by the first-order structural phase transition. Additionally, the $R\bar{3}m$ phase in other similar A_2B_3-type chalcogenides, such as Bi_2Se_3, Bi_2Te_3 and In_2Se_3, also underwent a pressure-induced metallization, so it may be a general physical phenomenon for most A_2B_3-type compounds.[34–36]

First-principles theoretical calculations based on DFT were carried out to further check changes in the crystalline and electronic structure for Ga_2S_3 under high pressure. Fig. 6a–c displays the calculated bandgap energy as a function of pressure, and the total and projected density states for Ga_2S_3 at 0 and 10 GPa, respectively. At ambient pressure, a wide energy gap existed between the valence bands (VB) and conduction bands (CB), and the calculated band gap is 1.725 eV, which shows typical semiconductor characterization. When the pressure was increased to 10 GPa, the band gap was 0 eV and an obvious overlap existed between the valence and conduction bands, which

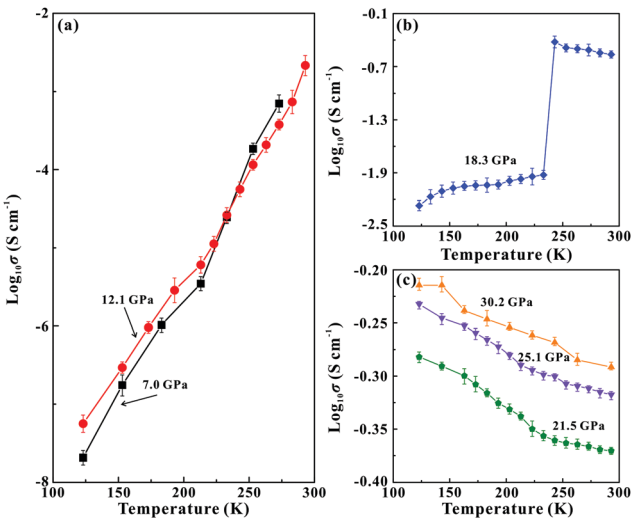

Fig. 5 (a) The temperature dependence of electrical conductivity for Ga_2S_3 at 7.0 and 12.1 GPa. (b) The evolution of electrical conductivity as a function of temperature at 18.3 GPa. (c) The temperature–electrical conductivity curves at 21.5, 25.1 and 30.2 GPa.

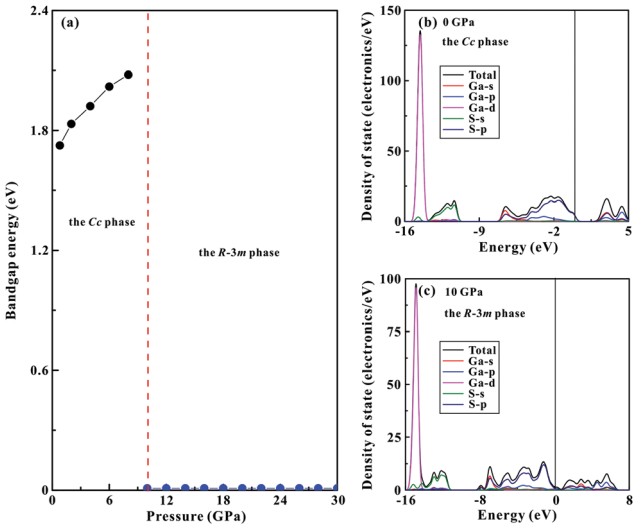

Fig. 6 (a) The bandgap energy of Ga_2S_3 with increasing pressure of up to 30 GPa from the first-principles calculations. (b) The density of state in the *Cc* phase of Ga_2S_3 at 0 GPa. (c) The density of state for the $R\bar{3}m$ phase at 10 GPa.

implies the occurrence of semiconductor-to-metal transition. The predicted metallization point is lower by nearly 7 GPa compared with our experimental data, which may be caused by an underestimation of bandgap energy by the GGA function.

Fig. 7a plots the enthalpies of the rhombohedral phase ($R\bar{3}m$) relative to the monoclinic phase (*Cc*) with an increase in pressure. The monoclinic *Cc* phase had the lowest enthalpy under ambient conditions and remained stable up to 13.2 GPa. Once the pressure exceeded 13.2 GPa, the rhombohedral $R\bar{3}m$ phase became more stable, which indicates that the *Cc* phase

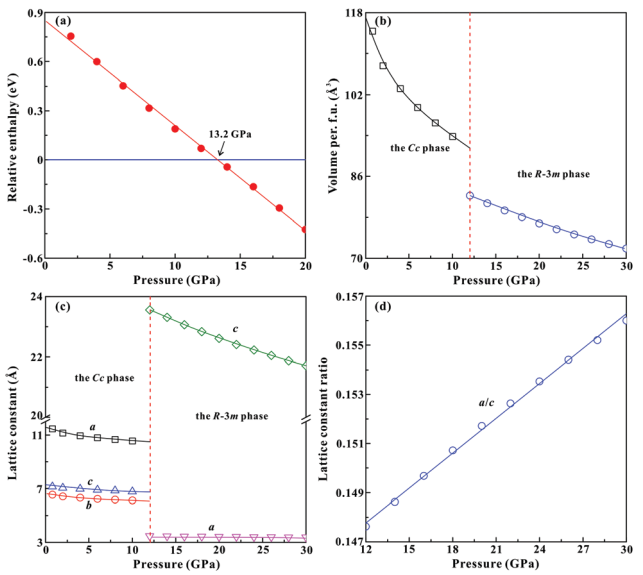

Fig. 7 (a) The enthalpy difference between the *Cc* phase and $R\bar{3}m$ phase as a function of pressure. (b) The volume in the unit cell of two phases as a function of pressure. (c) The calculated lattice parameters including *a*, *b* and *c* axes in the *Cc* phase and $R\bar{3}m$ phase. (d) The theoretical results of the pressure dependence of the *a*/*c* ratio at 12–30 GPa.

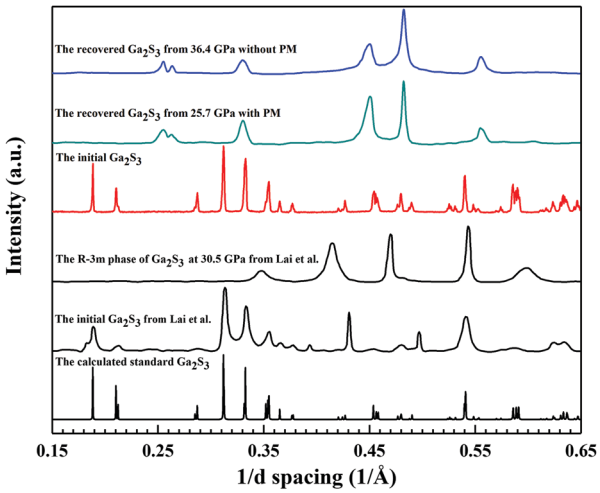

Fig. 8 The representative X-ray diffraction patterns of samples for the correspondent initial Ga_2S_3 (red color), and the recovered Ga_2S_3 from high pressure under different hydrostatic environments (green and blue colors). Here, the calculated standard Ga_2S_3 is also presented by virtue of the lattice parameters from Jones *et al.*[37] using the classic VESTA software from Momma and Izumi.[38] Previously reported X-ray diffraction results[17] on the initial and its corresponding high-pressure phase for Ga_2S_3 are also compared in detail.

transforms to the rhombohedral $R\bar{3}m$ phase at 13.2 GPa. After this transition, the unit cell volume sharply decreased by nearly 12.3%, which confirms that this transformation belongs to a first-order transition (Fig. 7b). The predicted point for the structural phase transition is comparable to that of the semiconductor-to-metal transition, and thus, we believe that the metallization is triggered by the first-order structural phase transition. The pressure dependence of the lattice parameters including the length of the *a*, *b* and *c* axes is presented in Fig. 7c. In the monoclinic *Cc* phase, the *a* axis had the largest compressibility, whereas the *c* axis had the largest compressibility in the rhombohedral $R\bar{3}m$ phase.

To examine whether the ETT occurs in the $R\bar{3}m$ phase of Ga_2S_3, the *a*/*c* ratio was calculated as plotted in Fig. 7d. Recent investigations on Bi_2Te_3 and Bi_2Se_3 have indicated that the ETT can induce pronounced changes in the *a*/*c* ratio.[8,19] However, we did not observe anomalies in the *a*/*c* ratio in the rhombohedral $R\bar{3}m$ phase of Ga_2S_3 from 12 GPa to 30 GPa, which indicates the absence of the ETT in the $R\bar{3}m$ phase of Ga_2S_3. We think that the metallic characterization in the $R\bar{3}m$ phase of Ga_2S_3 may account for the absence of ETT. It is believed that the topological property would disappear once metallization occurs owing to the full metallic bulk state.[34,35]

The occurrence of two possible new phases upon decompression is an interesting and unique physiochemical phenomenon for Ga_2S_3. To further confirm this observation, we performed X-ray diffraction experiment on the initial Ga_2S_3, and the recovered sample from a high pressure under different hydrostatic environments. As shown in Fig. 8, the XRD pattern of the initial sample was almost identical to that of the calculated standard Ga_2S_3, and also comparable to that of the initial Ga_2S_3 from Lai *et al.*[17] under ambient conditions.

The recovered samples are similar under different hydrostatic environments, whereas, they are totally different with the XRD patterns of the initial sample and the *in situ* high-pressure phase for Ga_2S_3 from Lai *et al.*[17] All of these obtained XRD results indicate that the recovered samples belong to a new phase with several different characteristic peaks.

Conclusions

The high-pressure behaviours of Ga_2S_3 were studied in different pressure environments up to 36.4 GPa by multiple experimental measurements combined with DFT calculations. Under non-hydrostatic conditions, a first-order structural phase transition existed in Ga_2S_3 at 17.2 GPa upon compression, which was characterized by anomalies in the pressure dependence of the Raman peaks, electrical conductivity, enthalpy energy and lattice parameters. This structural phase transition led to a semiconductor-to-metal transformation, which was confirmed by the temperature-dependent electrical conductivity measurements. Under hydrostatic conditions, similar structural phase transition and metallization were also observed but the transition pressure point was lower by 5.9 GPa. Upon decompression, the metallic Ga_2S_3 with the rhombohedral $R\bar{3}m$ structure underwent two possible structural phase transitions under both non-hydrostatic and hydrostatic conditions. No evidence showed the presence of the ETT in the $R\bar{3}m$ phase of Ga_2S_3.

Author contributions

L. D. and H. H. conceived the project, planned and organized experiments, and analysed the data. L. Y. and J. J. performed the electrical conductivity and Raman scattering measurements, and drafted the manuscript. M. H., X. Z. and H. L. carried out the HRTEM and X-ray diffraction analysis. L. D. and H. H. finalized the manuscript. P. L. explained the first-principles theoretical calculations.

Conflicts of interest

There are no conflicts to declare.

Acknowledgements

This research was financially supported by the NSF of China (42072055, 41772042 and 41774099) and the West Light Foundation of the Chinese Academy of Sciences and Youth Innovation Promotion Association of CAS (2019390). The support from the Supercomputer Center of Fujian Institute of Research on the Structure of Matter (FJIRSM) is acknowledged.

References

1 H. Zhang, C.-X. Liu, X.-L. Qi, X. Dai, Z. Fang and S.-C. Zhang, Topological insulators in Bi_2Se_3, Bi_2Te_3 and Sb_2Te_3 with a single Dirac cone on the surface, *Nat. Phys.*, 2009, **5**, 438–442.

2 P. Orgiani, C. Bigi, P. Kumar Das, J. Fujii, R. Ciancio, B. Gobaut, A. Galdi, C. Sacco, L. Maritato, P. Torelli, G. Panaccione, I. Vobornik and G. Rossi, Structural and electronic properties of Bi_2Se_3 topological insulator thin films grown by pulsed laser deposition, *Appl. Phys. Lett.*, 2017, **110**, 171601.

3 Y. L. Chen, J. G. Analytis, J.-H. Chu, Z. K. Liu, S.-K. Mo, X. L. Qi, H. J. Zhang, D. H. Lu, X. Dai, Z. Fang, S. C. Zhang, I. R. Fisher, Z. Hussain and Z.-X. Shen, Experimental realization of a three-dimensional topological insulator, Bi_2Te_3, *Science*, 2009, **325**, 178–181.

4 D. Hsieh, Y. Xia, D. Qian, L. Wray, F. Meier, J. H. Dil, J. Osterwalder, L. Patthey, A. V. Fedorov, H. Lin, A. Bansil, D. Grauer, Y. S. Hor, R. J. Cava and M. Z. Hasan, Observation of time-reversal-protected single-Dirac-cone topological-insulator states in Bi_2Te_3 and Sb_2Te_3, *Phys. Rev. Lett.*, 2009, **103**, 146401.

5 Y. Yang, Z. Xu, L. Sheng, R. Shen and D. Y. Xing, Magnetoresistance in an ultrathin Bi_2Se_3 film between two ferromagnetic insulators, *Appl. Phys. Lett.*, 2011, **99**, 182101.

6 C. Nayak, S. H. Simon, A. Stern, M. Freedman and S. Das, Sarma, Non-abelian anyons and topological quantum computation, *Rev. Mod. Phys.*, 2008, **80**, 1083–1159.

7 X. Hong, M. Newville, Y. Ding, T. Irifune, G. Gu and H.-K. Mao, Distinct intermediate states in the isostructural *R*-3*m* phase of the topological insulator Bi_2Se_3 at high pressure, *Phys. Rev. B*, 2020, **101**, 214107.

8 R. Vilaplana, D. Santamaría-Pérez, O. Gomis, F. J. Manjón, J. González, A. Segura, A. Muñoz, P. Rodríguez-Hernández, E. Pérez-González, V. Marín-Borrás, V. Muñoz-Sanjose, C. Drasar and V. Kucek, Structural and vibrational study of Bi_2Se_3 under high pressure, *Phys. Rev. B: Condens. Matter Mater. Phys.*, 2011, **84**, 184110.

9 K. Kirshenbaum, P. S. Syers, A. P. Hope, N. P. Butch, J. R. Jeffries, S. T. Weir, J. J. Hamlin, M. B. Maple, Y. K. Vohra and J. Paglione, Pressure-induced unconventional superconducting phase in the topological insulator Bi_2Se_3, *Phys. Rev. Lett.*, 2013, **111**, 087001.

10 K. Matsubayashi, T. Terai, J. S. Zhou and Y. Uwatoko, Superconductivity in the topological insulator Bi_2Te_3 under hydrostatic pressure, *Phys. Rev. B: Condens. Matter Mater. Phys.*, 2014, **90**, 125126.

11 J. Zhu, J. L. Zhang, P. P. Kong, S. J. Zhang, X. H. Yu, J. L. Zhu, Q. Q. Liu, X. Li, R. C. Yu, R. Ahuja, W. G. Yang, G. Y. Shen, H. K. Mao, H. M. Weng, X. Dai, Z. Fang, Y. S. Zhao and C. Q. Jin, Superconductivity in topological insulator Sb_2Te_3 induced by pressure, *Sci. Rep.*, 2013, **3**, 2016.

12 J. Ibáñez, J. A. Sans, C. Popescu, J. López-Vidrier, J. J. Elvira-Betanzos, V. P. Cuenca-Gotor, O. Gomis, F. J. Manjón, P. Rodríguez-Hernández and A. Muñoz, Structural, vibrational, and electronic study of Sb_2S_3 at high pressure, *J. Phys. Chem. C*, 2016, **120**, 10547–10558.

13 I. Efthimiopoulos, J. Zhang, M. Kucway, C. Park, R. C. Ewing and Y. Wang, Sb_2Se_3 under pressure, *Sci. Rep.*, 2013, **3**, 2665.

14 I. Efthimiopoulos, J. Kemichick, X. Zhou, S. V. Khare, D. Ikuta and Y. Wang, High-pressure studies of Bi_2S_3, *J. Phys. Chem. A*, 2014, **118**, 1713–1720.
15 I. Efthimiopoulos, C. Buchan and Y. Wang, Structural properties of Sb_2S_3 under pressure: evidence of an electronic topological transition, *Sci. Rep.*, 2016, **6**, 24246.
16 M.-J. Zhang, X.-M. Jiang, L.-J. Zhou and G.-C. Guo, Two phases of Ga_2S_3: promising infrared second-order nonlinear optical materials with very high laser induced damage thresholds, *J. Mater. Chem. C*, 2013, **1**, 4754.
17 X. Lai, F. Zhu, S. Qin, D. Chen, Y. Li, K. Yang and X. Wu, Experimental and theoretical identification of a high-pressure polymorph of Ga_2S_3 with α-Bi_2Te_3-type structure, *J. Appl. Phys.*, 2014, **116**, 193507.
18 A. Bera, K. Pal, D. V. S. Muthu, U. V. Waghmare and A. K. Sood, Pressure-induced phase transition in Bi_2Se_3 at 3 GPa: electronic topological transition or not?, *J. Phys.: Condens. Matter*, 2016, **28**, 105401.
19 A. Polian, M. Gauthier, S. M. Souza, D. M. Trichês, J. C. de Lima and T. A. Grandi, Two-dimensional pressure-induced electronic topological transition in Bi_2Te_3, *Phys. Rev. B: Condens. Matter Mater. Phys.*, 2011, **83**, 113106.
20 J. Zhang, T. Hu, J. Yan, F. Ke, J. Wang, X. Cui, X. Li, Y. Ma, J. Yang and C. Gao, Pressure driven semi-metallic phase transition of Sb_2Te_3, *Mater. Lett.*, 2017, **209**, 78–81.
21 L. Dai, Y. Zhuang, H. Li, L. Wu, H. Hu, K. Liu, L. Yang and C. Pu, Pressure-induced irreversible amorphization and metallization with a structural phase transition in arsenic telluride, *J. Mater. Chem. C*, 2017, **5**, 12157–12162.
22 H. K. Mao, J. Xu and P. M. Bell, Calibration of the ruby pressure gauge to 800 kbar under quasi-hydrostatic conditions, *J. Geophys. Res.*, 1986, **91**, 4673–4676.
23 L. Dai, L. Wu, H. Li, H. Hu, Y. Zhuang and K. Liu, Pressure-induced phase-transition and improvement of the microdielectric properties in yttrium-doped $SrZrO_3$, *Europhys. Lett.*, 2016, **114**, 56003.
24 L. Dai, L. Wu, H. Li, H. Hu, Y. Zhuang and K. Liu, Evidence of the pressure-induced conductivity switching of yttrium-doped $SrTiO_3$, *J. Phys.: Condens. Matter*, 2016, **28**, 475501.
25 L. Dai, K. Liu, H. Li, L. Wu, H. Hu, Y. Zhuang, L. Yang, C. Pu and P. Liu, Pressure-induced irreversible metallization accompanying the phase transitions in Sb_2S_3, *Phys. Rev. B*, 2018, **97**, 024103.
26 L. Dai, C. Pu, H. Li, H. Hu, K. Liu, L. Yang and M. Hong, Characterization of metallization and amorphization for GaP under different hydrostatic environments in diamond anvil cell up to 40.0 GPa, *Rev. Sci. Instrum.*, 2019, **90**, 066103.
27 L. Yang, L. Dai, H. Li, H. Hu, K. Liu, C. Pu, M. Hong and P. Liu, Pressure-induced metallization in $MoSe_2$ under different pressure conditions, *RSC Adv.*, 2019, **9**, 5794–5803.
28 Y. Zhuang, L. Dai, L. Wu, H. Li, H. Hu, K. Liu, L. Yang and C. Pu, Pressure-induced permanent metallization with reversible structural transition in molybdenum disulfide, *Appl. Phys. Lett.*, 2017, **110**, 122103.
29 C.-H. Ho, M.-H. Lin, Y.-P. Wang and Y.-S. Huang, Synthesis of In_2S_3 and Ga_2S_3 crystals for oxygen sensing and UV photodetection, *Sens. Actuators, A*, 2016, **245**, 119–126.
30 C. Julien, S. Barnier, I. Ivanov, M. Guittard, M. P. Pardo and A. Chilouet, Vibrational studies of copper thiogallate solid solutions, *Mater. Sci. Eng., B*, 1999, **57**, 102–109.
31 F. J. Manjón, R. Vilaplana, O. Gomis, E. Pérez-González, D. Santamaría-Pérez, V. Marín-Borrás, A. Segura, J. González, P. Rodríguez-Hernández, A. Muñoz, C. Drasar, V. Kucek and V. Muñoz-Sanjosé, High-pressure studies of topological insulators Bi_2Se_3, Bi_2Te_3, and Sb_2Te_3, *Phys. Status Solidi B*, 2013, **250**, 669–676.
32 O. Gomis, R. Vilaplana, F. J. Manjón, P. Rodríguez-Hernández, E. Pérez-González, A. Muñoz, V. Kucek and C. Drasar, Lattice dynamics of Sb_2Te_3 at high pressures, *Phys. Rev. B: Condens. Matter Mater. Phys.*, 2011, **84**, 174305.
33 X.-M. Zhao, H. Liu, A. F. Goncharov, Z.-W. Zhao, V. V. Struzhkin, H.-K. Mao, A. G. Gavriliuk and X.-J. Chen, Pressure effect on the electronic, structural, and vibrational properties of layered 2*H*-$MoTe_2$, *Phys. Rev. B*, 2019, **99**, 024111.
34 J. Zhang, Y. Han, C. Liu, X. Zhang, F. Ke, G. Peng, Y. Ma, Y. Ma and C. Gao, Semiconductor-to-metal transition of Bi_2Se_3 under high pressure, *Appl. Phys. Lett.*, 2014, **105**, 062102.
35 J. Zhang, C. Liu, X. Zhang, F. Ke, Y. Han, G. Peng, Y. Ma and C. Gao, Electronic topological transition and semiconductor-to-metal conversion of Bi_2Te_3 under high pressure, *Appl. Phys. Lett.*, 2013, **103**, 052102.
36 J. Zhao and L. Yang, Structure evolutions and metallic transitions in In_2Se_3 under high pressure, *J. Phys. Chem. C*, 2014, **118**, 5445–5452.
37 C. Y. Jones, J. C. Bryan, K. Kirschbaum and J. G. Edwards, Refinement of the crystal structure of digallium trisulfide, G_2S_3, *Z. Kristallogr. – New Cryst. Struct.*, 2001, **216**, 327–328.
38 K. Momma and F. Izumi, VESTA: a three-dimensional visualization system for electronic and structural analysis, *J. Appl. Crystallogr.*, 2008, **41**, 653–658.

